minerals

Article

Caledonian Tin Mineralization in the Jiuwandashan Area, Northern Guangxi, South China

Zhi-Heng Yue [1,2], Ling-An Bai [1,2,*], Rong-Guo Hu [1,2,*], Jie Wu [1,2], Yu Dai [3], Shou-Yu Zhou [4], Zuo-Hai Feng [1,2], Cheng Xu [1,2], Zeng-Xia Zhao [1,2] and Xi-Jun Liu [1,2]

1 College of Earth Sciences, Guilin University of Technology, Guilin 541004, China; yzh15610902919@163.com (Z.-H.Y.); wujie@glut.edu.cn (J.W.); fzh@glut.edu.cn (Z.-H.F.); xucheng1999@pku.edu.cn (C.X.); zhaozx@glut.edu.cn (Z.-X.Z.); xijunliu@glut.edu.cn (X.-J.L.)
2 Collaborative Innovation Center for Exploration of Nonferrous Metal Deposits and Efficient Utilization of Resources in Guangxi, Guilin University of Technology, Guilin 541004, China
3 Guangxi Institute of Regional Geological Survey, Guilin 541004, China; yudai@glut.edu.cn.com
4 China Nonferrous Metal (Guilin) Geology and Mining Co., Ltd., Guilin 541004, China; shouyuzhou@163.com
* Correspondence: bailingan@glut.edu.cn (L.-A.B.); hurongguo@glut.edu.cn (R.-G.H.)

Abstract: The Jiangnan orogenic belt is located between the Yangtze and Cathaysia blocks in South China and is one of the largest W–Sn–Nb–Ta ore belts worldwide. Mineralization occurred from the Proterozoic to Mesozoic, but Caledonian Sn mineralization has rarely been reported. The Jialong cassiterite–sulfide deposit is located in the western Jiangnan orogenic belt. It is hosted by the Sibao Group and in contact with the northeastern part of the Yuanbaoshan granite. The deposit was overprinted by the Sirong ductile shear zone. Here, we present cassiterite U–Pb and mylonitic granite muscovite $^{40}Ar/^{39}Ar$ ages for this deposit. The cassiterite and muscovite yielded concordant U–Pb and $^{40}Ar/^{39}Ar$ ages of 422–420 Ma, indicating that Sn mineralization occurred during the early Paleozoic and was spatially and temporally related to the ductile shear zone. The cassiterite is depleted in Nb (0.51–5.46 ppm), Ta (0.01–1.09 ppm), Ti (32.84–423.15 ppm), Sc (0.02–1.45 ppm), Hf (0–1.11 ppm), and other high-field-strength elements. Elements, such as Pb (0.01–8.11 ppm) and Sb (9.92–56.45 ppm), are relatively enriched in the cassiterite, which indicate the Jialong deposit was not directly related to magmatism. Shearing along the Sirong ductile shear zone occurred at 419.6 ± 3.8 Ma, concurrent with the formation of the Jialong Sn–Cu deposit. Moreover, cassiterite in the deposit exhibits obvious shear and brittle deformation, and dissolution and regrowth, suggesting that Sn mineralization was closely related to ductile shearing. The Sirong ductile shear zone and secondary shear structures had a key role in controlling the Sn orebody. The heat generated during tectonic deformation in the ductile shear zone may have produced the ore-forming hydrothermal fluids, and NW–SE-trending fractures in the strata provided the space for mineralization. Metamorphic hydrothermal fluids generated by Caledonian shear deformation extracted Sn from Sn-rich strata, which then migrated along interlayer fractures produced by shearing. A decrease in pressure and water–rock reactions led to the mineralization of Sn and other elements. This deposit is the first example of Caledonian and shear zone-related Sn mineralization identified in the Jiuwandashan area of northern Guangxi.

Keywords: Jiuwandashan; U–Pb age; $^{40}Ar/^{39}Ar$ age; Sirong ductile shear; Caledonian; Jialong Sn–Cu deposit

Citation: Yue, Z.-H.; Bai, L.-A.; Hu, R.-G.; Wu, J.; Dai, Y.; Zhou, S.-Y.; Feng, Z.-H.; Xu, C.; Zhao, Z.-X.; Liu, X.-J. Caledonian Tin Mineralization in the Jiuwandashan Area, Northern Guangxi, South China. *Minerals* **2022**, *12*, 843. https://doi.org/10.3390/min12070843

Academic Editor: Manuel Francisco Pereira

Received: 16 June 2022
Accepted: 27 June 2022
Published: 30 June 2022

1. Introduction

Most Sn deposits globally are directly or indirectly related to highly differentiated S-type biotite granites [1–3], but there are also some deposits that are unrelated to granites. For example, the Kafang Sn deposit in Gejiu in Yunnan Province of China [4] occurs in the interior of a basalt lava flow and along the contact zone between basalt and surrounding rocks. The Yunlong Sn deposit in Yunnan Province has a metamorphic origin [5], and the Neves Corvo Sn–Cu–polymetallic deposit in Portugal is a submarine sedimentary–exhalative deposit [6–8]. There have been few studies on Sn mineralization that has no direct relationships to granite, which partially hinders exploration for Sn ore.

Tin deposits in China are mainly located in South China (Nanling and adjacent areas), apart from the middle and lower reaches of the Yangtze River and southeastern coastal areas, and especially in the Jiangnan orogenic belt [9–13]. Jiuwandashan is located in the northern Guangxi–Zhuang Autonomous Region in the western Jiangnan orogenic belt. It is located adjacent to the Dachang super-large Sn ore field in the west and the Limu and Shanhu Sn deposits in the east. Tin–polymetallic deposits or mineralization is widely scattered throughout this region. In addition to two large Sn deposits at Jiumao and Yidong, >20 small- and medium-sized Sn deposits are developed in this region. Neoproterozoic strata are widely exposed in this area, which was also affected by intense Neoproterozoic magmatism. The Sibao Group is Sn-rich, with an average Sn content of 13.1 ppm [14], Sn content of 2.1 ppm in the upper crust and that in the sedimentary rocks of South China is 3.4 ppm [15]. NNE–SSW-trending faults and ductile shear zones are well developed throughout the study area [16]. Tin mineralization is spatially and temporally related to Neoproterozoic silicic–mafic–ultramafic igneous rocks, and also metamorphic rocks and the ductile shear zone in the Sibao Group [17]. However, Sn mineralization occurred mainly during the Neoproterozoic, and there have been no reports of Sn mineralization at other times. It has been proposed that deformation and metamorphism during the Caledonian Orogeny led to the migration and mineralization of Sn in Neoproterozoic strata and mafic–ultramafic rocks [18]. It is also thought that Caledonian Sn deposits exist in northern Guangxi [18,19], but this has not been confirmed.

In this study, we conducted cassiterite U–Pb dating of the Jialong Sn–Cu deposit in the Jiuwandashan area, northern Guangxi, and demonstrate that Sn mineralization occurred in the early Paleozoic. Major and trace element data for cassiterite and mylonitic granite ^{40}Ar/^{39}Ar dating were also used to identify the source of the deposit. These data, and the close genetic relationship between the Sn mineralization and Caledonian ductile shear zone, are used to develop a mineralization model for Caledonian Sn mineralization in northern Guangxi, and elsewhere in South China, which provides new opportunities for Sn ore exploration.

2. Geological Background

The Jiangnan orogenic belt is located between the Yangtze and Cathaysia blocks, and is one of the most important W–Sn–Nb–Ta mineralization belts worldwide (Figure 1a). The study area is located in northern Guangxi in the western Jiangnan orogenic belt. The strata comprise mainly clastic rocks of the early Neoproterozoic Sibao and Danzhou groups, which record different grades of metamorphism. The region has experienced Sibao, Xuefeng, and Caledonian tectonism. This led to the development of deep and large faults with variable trends and shear zones. From west to east, these are the Jiufeng, Motianling, Sibao, Yuanbaoshan, and Sirong shear zones. The Sirong ductile shear zone is located on the eastern side of the Yuanbaoshan biotite-granite pluton and has a length of >40 km and a width of 1.5–5.0 km. It is a large dextral strike-slip and thrust ductile shear zone that strikes 250–300° and dips 45–70° to the NWW. In the interior of the shear zone, the strata are highly schistose, the granite is strongly mylonitized, and ductile deformation structures are developed, including mylonitic and tensile lineations, and quartz augens have frequently occurred in the study area, including mafic-ultramafic magmatism, and the Motianling and Yuanbaoshan granitic plutons. Magmatism occurred mainly during the middle Neoproterozoic (*ca*. 855–820 Ma) [20–28].

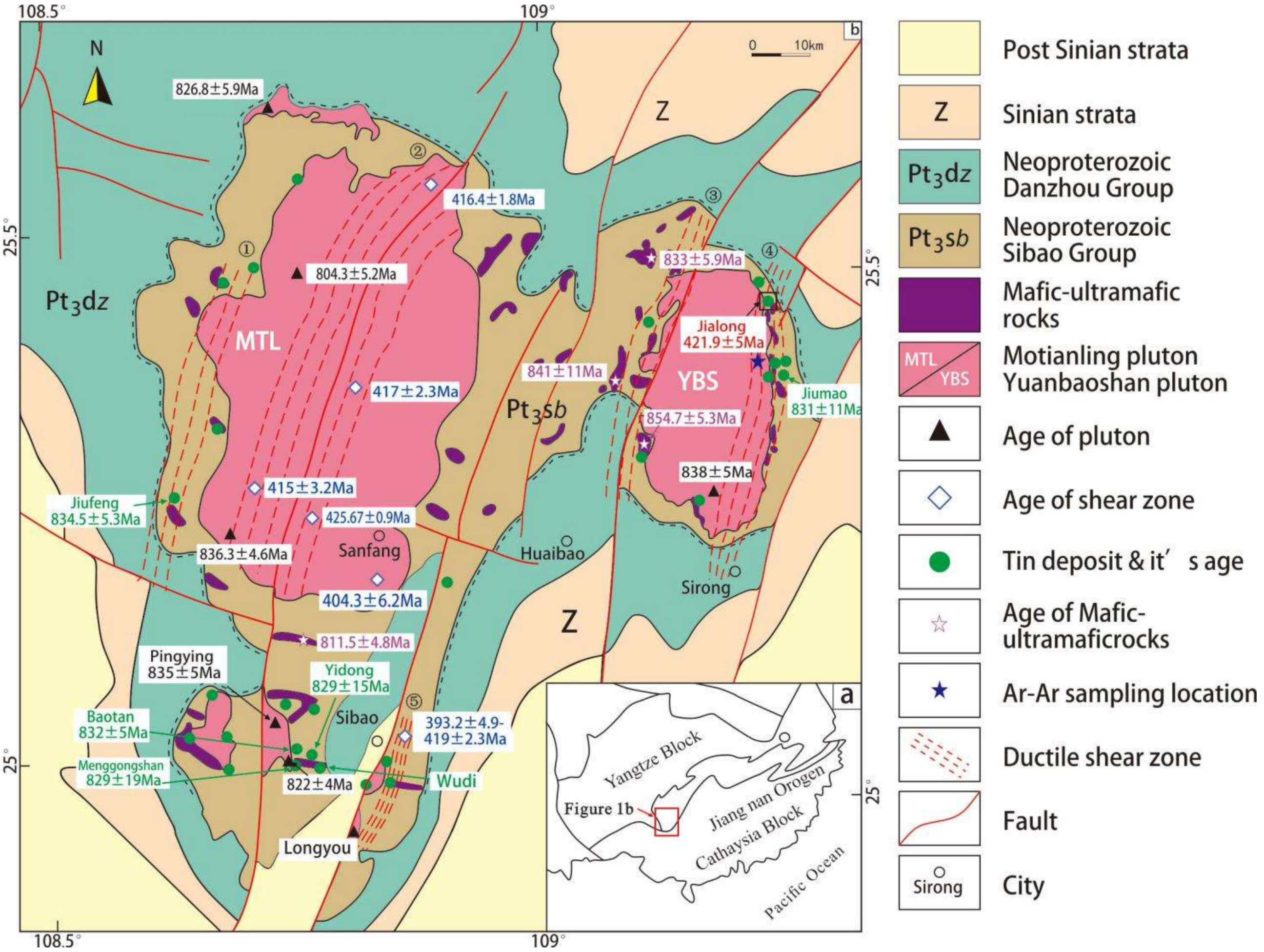

Figure 1. (**a**) Geological sketch of South China; (**b**) sketch map of the geology and distribution of Sn ore deposits in northern Guangxi [18,22,26,28–32] (modified after Mao, 1988; Wang et al., 2006; Zhang et al., 2019; Li et al., 2020, age data are referenced). Major shear zones: ① Jiufeng ductile shear zone (modified after Dai et al., 2020); ② Motianling ductile shear zone (modified after Zhang, 2004); ③ Yuanbaoshan ductile shear zone (modified after Zhang, 2004; Guo, 2017); ④ Sirong ductile shear zone (modified after Zhang, 2004; Guo, 2017); ⑤ Sibao ductile shear zone (modified after Zhang et al., 2015).

3. Geology of the Jialong Tin Deposit

The Jialong deposit is a vein cassiterite–sulfide deposit, located at the contact between the Sirong ductile shear zone and northeastern part of the Neoproterozoic Yuanbaoshan granitic pluton. The deposit was discovered in the 1960s and has proven reserves of 9561 tons of Cu and 3848 tons of Sn, and is still being mined (Bureau of Geology and Mineral Resources of Guangxi Province). In the mining area, only the Yuxi Formation of the Sibao Group (Pt_3y) and Baizhu Formation of the Danzhou Group (Pt_3b) are exposed. The Yuxi Formation consists of muscovite–quartz schist intercalated with granulite and two-mica–quartz schist. These rocks have experienced silicification and chloritization, and Cu–Sn orebodies are present in the upper part of the formation. The Baizhu Formation consists of muscovite–quartz schist intercalated with granulite and calcareous schist.

Folds and faults are well developed in the mining area. The Yuxi Formation at the margin of the Yuanbaoshan granitic pluton is strongly deformed by a series of small reverse and interlayer drag folds. NE–SW-trending compression–shear faults are also developed but are small in scale (2–3 km long). A small number of NW–SE-trending faults are observed in the mining area.

The Yuanbaoshan granitic pluton is a N–S-trending, elliptically shaped batholith that intrudes the Yuxi Formation and yields an age of 838 ± 5 Ma [33]. In addition, there are five NW–SE-trending gabbroic dikes in the mining area, which are thought to be Neoproterozoic in age, although precise ages are not available for these rocks. The dikes are 10 to >100 m long (Figure 2).

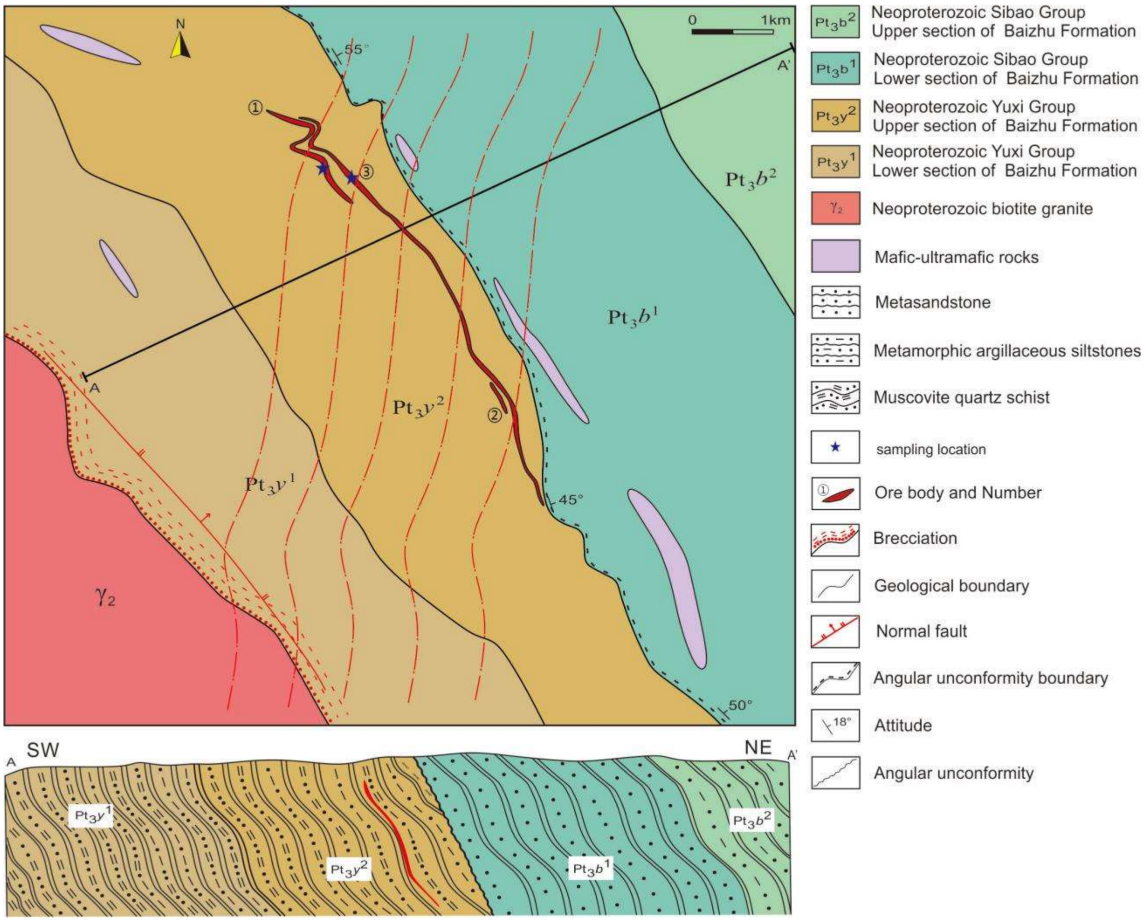

Figure 2. Geological map of the Jialong Cu–Sn deposit [16] (modified after Bureau of Geology and Mineral Resources of Guangxi Province).

The orebody is controlled by the layering in the host rocks and occurs mainly in silicified quartz schist of the Yuxi Formation (Figure 2). Eleven veins occur in the mining area, which mostly have arc-like, wavy, lamellar, lens-like, and lenticular shapes (Figure 2). The veins are 20–700 m long, 0.7–9.3 m thick, dip 40–60°, and have a Sn grade of 0.2–0.3 wt.%.

The ore is mainly disseminated, but there is also a small amount of massive, vein, and banded ores. The main ore minerals are chalcopyrite, cassiterite, arsenopyrite, pyrite, and pyrrhotite, along with lesser sphalerite, marcasite, and stibnite (Figure 3g). Chalcopyrite has an allotriomorphic granular texture (Figure 3i) and is typically associated with cassiterite, pyrrhotite, pyrite, and arsenopyrite (Figure 3g). The cassiterite in the Jialong deposit is fine grained and typically associated with sulfide minerals (e.g., pyrrhotite) and quartz. Cassiterite occurs as equant grains and scarce long columnar crystals. Metasomatic dissolution and fracturing of cassiterite is common (Figure 3f,h). The gangue minerals are mainly quartz, along with lesser muscovite, chlorite, biotite, tourmaline, and plagioclase. The Jialong deposit can be divided into three mineralization stages: the cassiterite–silicate, cassiterite–quartz, and cassiterite–sulfide stages. The alteration associated with mineralization includes mainly silicification, pyrrhotitization, and pyritization, in addition to lesser sericitization, chloritization, and tourmalization.

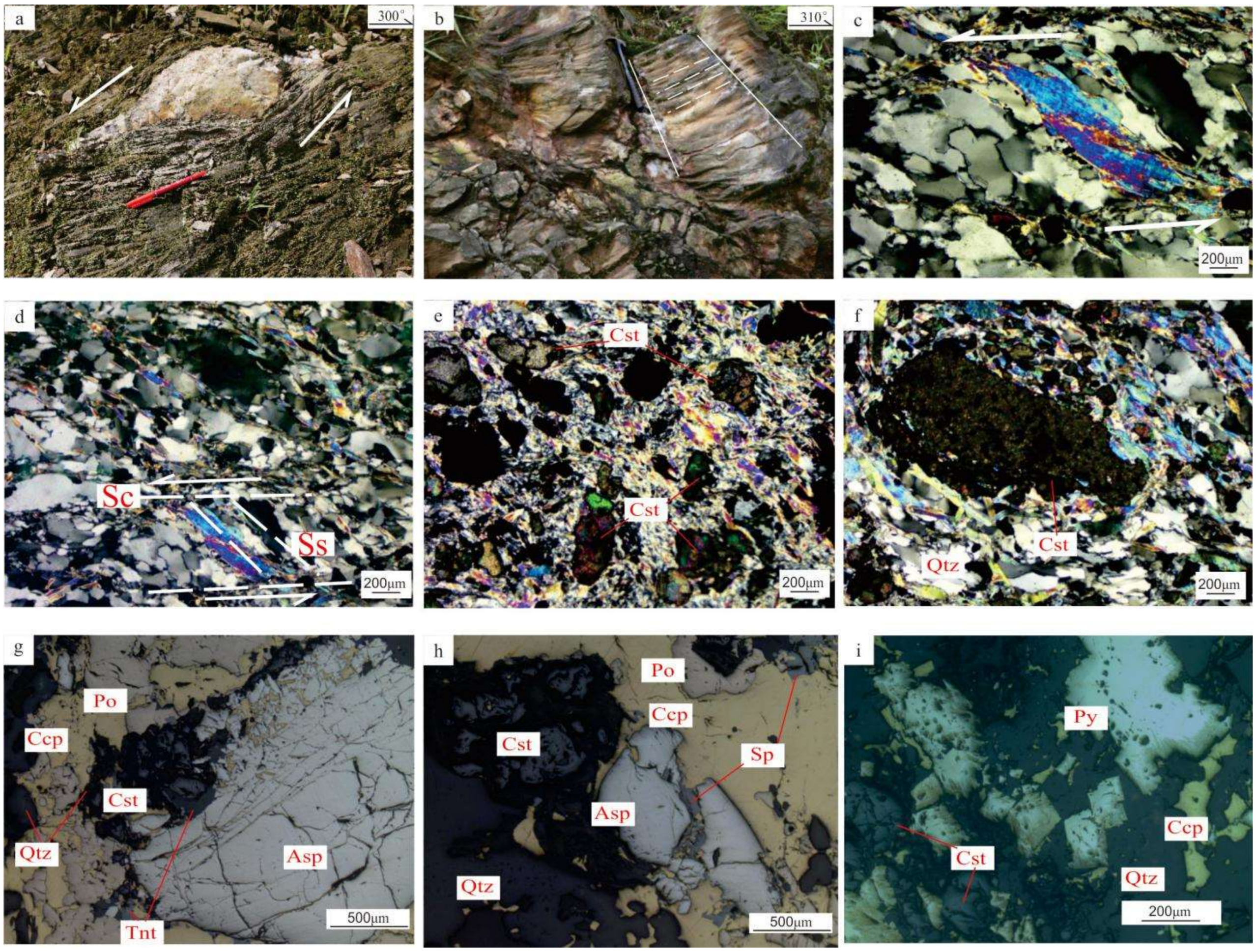

Figure 3. Photomicrographs of typical textures and mineral assemblages in the Jialong Sn–Cu deposit. (**a**) Ocellar quartz indicative of thrusting and shearing. (**b**) Schistosity plane with a folded lineation that was cut by late brittle fractures. (**c**) Mica fish indicative of ductile deformation and sinistral shear. (**d**) S–C fabric indicative of sinistral movement. (**e**) Fine-grained and patchily distributed cassiterite (Cst). (**f**) Patchy cassiterite surrounded by quartz (Qtz). (**g**) Dissolved (Ccp) chalcopyrite, (Tnt) tintinaite, fractured (Asp) arsenopyrite, cassiterite, and (Po) pyrrhotite. (**h**) Fractured arsenopyrite infilled by late (Sp) sphalerite. (**i**) Allotriomorphic granular (Py) pyrite associated with chalcopyrite and cassiterite.

4. Samples and Analytical Methods

Ore samples of the cassiterite–sulfide stage from the middle of the No. 3 vein were selected for U–Pb dating and trace element analysis of cassiterite. Mylonitic granite was collected from the northeastern margin of the Yuanbao Mountain Pluton. It consists mainly of quartz, plagioclase, K-feldspar, biotite, and muscovite, along with minor chlorite, tourmaline, apatite, and titanite. Preferred alignment of biotite and muscovite defines the mylonitic foliation. Quartz in the mylonite exhibits features typical of ductile deformation, including undulose extinction, dynamic recrystallization, and sub-grain rotation and recrystallization.

Cassiterite U–Pb dating was conducted at the State Key Laboratory of Deposit Geochemistry, Guiyang Institute of Geochemistry, Chinese Academy of Sciences, Guizhou, China. Dating was undertaken with an Agilent 7700× inductively coupled plasma mass spectrometer.

LA–ICP–MS trace element analysis of cassiterite was conducted at the State Key Laboratory of Mineral Deposit Geochemistry, Guiyang Institute of Geochemistry, Chinese

Academy of Sciences, Guiyang, China. These analyses were undertaken with an Agilent 7900 ICP–MS.

Argon isotope in biotite of mylonitized granite ratios were determined at the MOE Key Laboratory of Tectonics and Petroleum Resources, China University of Geosciences, Wuhan, China. Laser stepwise heating of samples was undertaken with a 50 W CO_2 laser, which was coupled to an ARGUS VI® noble gas mass spectrometer [34].

5. Results

5.1. Cassiterite U–Pb Ages

The cassiterite U–Pb dating results are listed in Table 1. The cassiterite can be divided into two types: (1) euhedral and pure cassiterite; and (2) anhedral cassiterite with rough surfaces, dissolution features, and numerous inclusions and deformation features. The latter was affected by hydrothermal alteration and/or deformation. In addition, cassiterite grains exhibit distinct oscillatory growth bands in back-scattered electron images (Figure 4).

Table 1. LA–ICP–MS U–Pb dating results for cassiterite in the Jialong Sn–Cu deposit.

Spot No.	Pb	U	Th	$^{207}Pb/^{206}Pb$		$^{207}Pb/^{235}U$		$^{206}Pb/^{238}U$		$^{207}Pb/^{206}Pb$		$^{207}Pb/^{235}U$		$^{206}Pb/^{238}U$	
		ppm		Ratio	1σ	Ratio	1σ	Ratio	1σ	Age (Ma)	1σ	Age (Ma)	1σ	Age (Ma)	1σ
JL01	0.081	0.217	0.552	0.26	0.022	2.972	0.261	0.083	0.003	3250.3	135.2	1400.7	66.9	519.9	18.87
JL02	0.098	0.033	1.07	0.142	0.112	1.381	0.101	0.072	0.002	2261.1	136.4	881.1	43.3	451.5	11.6
JL03	0.021	0.003	0.128	0.361	0.051	4.347	0.438	0.101	0.005	3755.2	219.9	1702.4	83.4	620.3	33.9
JL04	0.007	0.001	0.02	0.012	0.388	8.206	1.692	0.129	0.019	-	-	2254.1	186.7	785.3	113.3
JL05	0.404	0.012	5.902	0.071	0.005	0.683	0.046	0.069	0.001	953.7	140.7	529.0	28.3	432.3	4.8
JL06	0.776	0.027	0.339	0.412	0.036	5.999	0.415	0.114	0.004	3954.6	132.0	1975.7	60.3	700.0	25.1
JL07	0.017	0	0.157	0.223	0.029	2.156	0.254	0.073	0.004	3007.1	213.4	1167.0	81.9	452.4	24.6
JL08	0.044	0.002	0.569	0.082	0.01	0.79	0.09	0.07	0.002	1261.1	234.4	591.4	51.1	441.1	15.2
JL09	0.025	0.006	0.262	0.146	0.019	1.416	0.168	0.076	0.003	2310.2	227.5	896.1	70.9	477.4	19.0
JL10	0.025	0	0.294	0.202	0.028	1.724	0.208	0.069	0.003	2846.6	234.6	1017.6	77.8	434.0	20.4
JL11	0.101	0.034	1.381	0.074	0.007	0.697	0.069	0.069	0.001	1053.7	211.6	537.2	41.4	430.9	11.5
JL12	0.101	0.004	0.189	0.634	0.041	15.452	0.899	0.179	0.005	4588.6	95.5	2843.6	55.5	1062.8	30.5
JL13	0.161	0.001	2.579	0.057	0.004	0.508	0.036	0.063	0.001	520.4	169.4	417.2	24.9	397.2	8.4
JL14	0.114	0.001	1.62	0.076	0.007	0.716	0.066	0.069	0.001	1099.7	201.9	548.9	39.4	434.0	9.9
JL15	0.169	0.008	0.408	0.525	0.031	11.69	0.666	0.164	0.005	4313.4	89.1	2579.9	53.3	982.5	29.3
JL16	0.073	0	1.04	0.054	0.005	0.544	0.056	0.073	0.002	466.7	213.9	441.2	37.1	455.2	12.2
JL17	0.082	0.005	0.722	0.263	0.021	2.543	0.186	0.075	0.003	3268.2	129.3	1284.7	53.5	467.9	17.7
JL18	0.039	0.007	0.366	0.194	0.022	1.99	0.254	0.075	0.003	2778.7	194.9	1112.3	86.3	469.6	23.9
JL19	0.027	0	0.152	0.409	0.047	4.807	0.455	0.103	0.007	3944.4	176.4	1786.1	79.7	637.1	40.6
JL20	0.171	0.023	0.69	0.304	0.028	5.594	0.856	0.114	0.008	3495.4	143.8	1915.2	131.9	698.2	50.4
JL21	0.026	0	0.316	0.199	0.033	1.757	0.253	0.072	0.003	2820.4	275.0	1030.0	93.3	450.4	20.6
JL22	0.054	0.006	0.482	0.179	0.017	2.062	0.191	0.083	0.002	2650.9	162.5	1136.4	63.4	515.4	15.8
JL23	1.041	0.018	1.475	0.626	0.022	22.244	1.014	0.23	0.007	4570.1	51.8	3194.5	44.4	1339.6	36.9
JL24	0.107	0.003	1.444	0.073	0.006	0.731	0.057	0.07	0.001	1016.7	168.5	557.5	33.5	441.2	7.4
JL25	0.032	0	0.156	0.445	0.153	3.399	0.32	0.092	0.006	4069.4	540.4	1504.3	73.9	567.6	40.2
JL26	0.018	0	0.059	0.796	0.255	6.928	0.803	0.106	0.011	-	-	2102.4	102.9	651.8	66.0
JL27	0.061	0.003	0.343	0.319	0.025	6.928	0.803	0.106	0.011	3565.4	121.9	1799.4	71.9	689.1	27.7
JL28	0.052	0.007	0.152	0.48	0.052	7.802	0.775	0.123	0.004	4183.3	161.8	2208.5	89.5	748.8	27.4
JL29	0.025	0	0.289	0.167	0.04	1.386	0.236	0.079	0.003	2531.5	414.7	883.1	100.8	494.1	20.4
JL30	0.5	0	0.42	0.714	0.026	38.832	3.511	0.38	0.029	-	-	3741.4	89.6	2079.7	135.4
JL31	0.239	0	0.356	0.066	0.004	0.628	0.04	0.068	0.001	816.7	134.1	495.1	25.5	429.5	5.6
JL32	0.021	0.001	0.249	0.208	0.032	1.891	0.282	0.076	0.003	2891.1	255.3	1078.1	99.2	475.9	23.8
JL33	0.034	0	0.43	0.107	0.015	1.066	0.147	0.071	0.003	1753.7	268.5	737.1	72.5	443.7	18.2
JL34	0.087	0.002	1.134	0.08	0.006	0.831	0.067	0.073	0.001	1220.4	167.1	614.3	37.7	455.3	8.3
JL35	0.033	0.001	0.043	0.918	0.143	23.494	1.939	0.244	0.015	-	-	3247.7	80.4	1408.6	82.0
JL36	0.054	0.003	0.71	0.09	0.013	0.819	0.107	0.069	0.002	1438.9	277.8	608.0	60.2	432.5	13.6

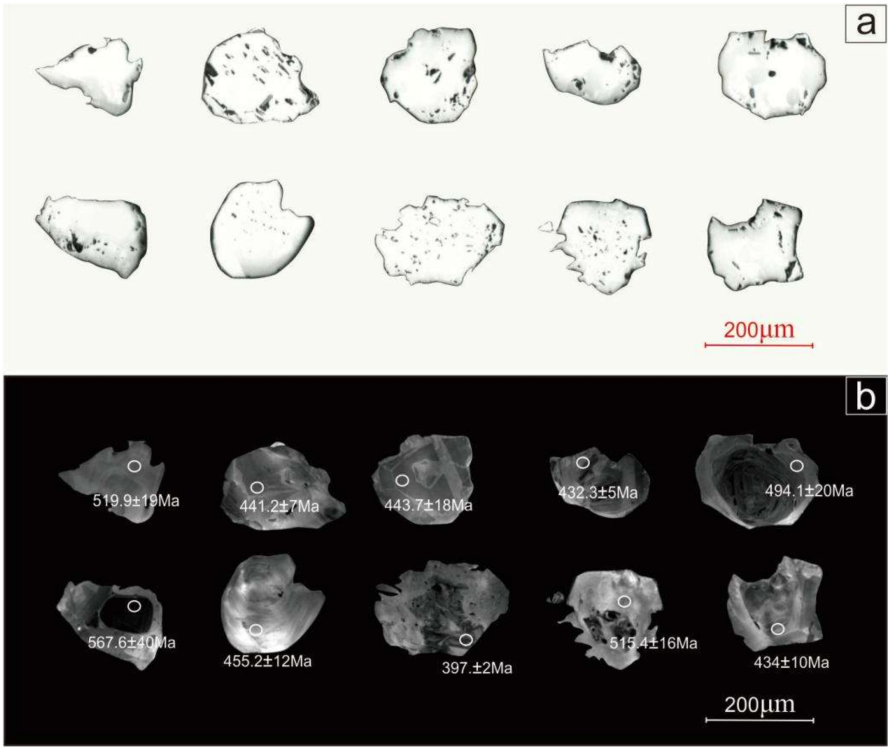

Figure 4. (**a**) Reflected light and (**b**) cathodoluminescence images of cassiterite in the Jialong Cu–Sn deposit.

Our results show that some cassiterite crystallized from hydrothermal fluids and has low U contents (U < 10 ppm), and, thus, the cassiterite rims record the timing of fluid dissolution and recrystallization, whereas the cores record the age of primary cassiterite formation [35]. There are no obvious differences between the U–Pb ages of cassiterite cores and rims. Thirty-six analyses yielded a concordant $^{207}Pb/^{206}Pb$–$^{238}U/^{206}Pb$ age of 421.9 ± 5.0 Ma (Figure 5), which indicates the Jialong Sn–Cu deposit formed during the early Paleozoic.

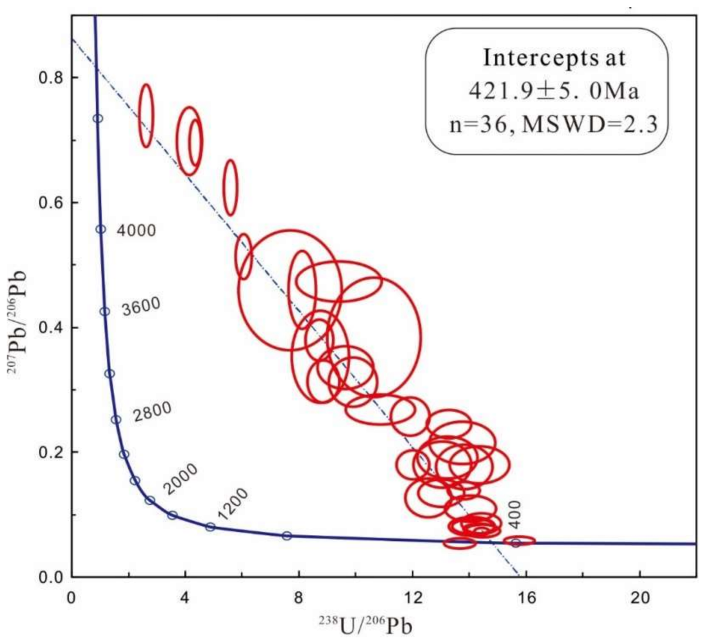

Figure 5. U–Pb concordia diagram for cassiterite from the Jialong Sn–Cu deposit.

5.2. $^{40}Ar/^{39}Ar$ Dating

Stepwise heating of biotite (18Y33Bt) from mylonitic granite yielded older apparent ages for the first two steps (446–428 Ma) and younger apparent ages for the last three steps (409–397 Ma). A flat age spectrum was formed by steps 3–11, which yielded a plateau age of 419.6 ± 3.8 Ma (MSWD = 0.3; ^{39}Ar = 85%; Figure 6). The inverse isochron age is 419.7 ± 3.8 Ma (MSWD = 0.3), with an initial $^{40}Ar/^{36}Ar$ ratio of 294 ± 35 (Figure 6). This is consistent with the plateau age. This age is the best estimate for the timing of deformation of the Sirong ductile shear zone.

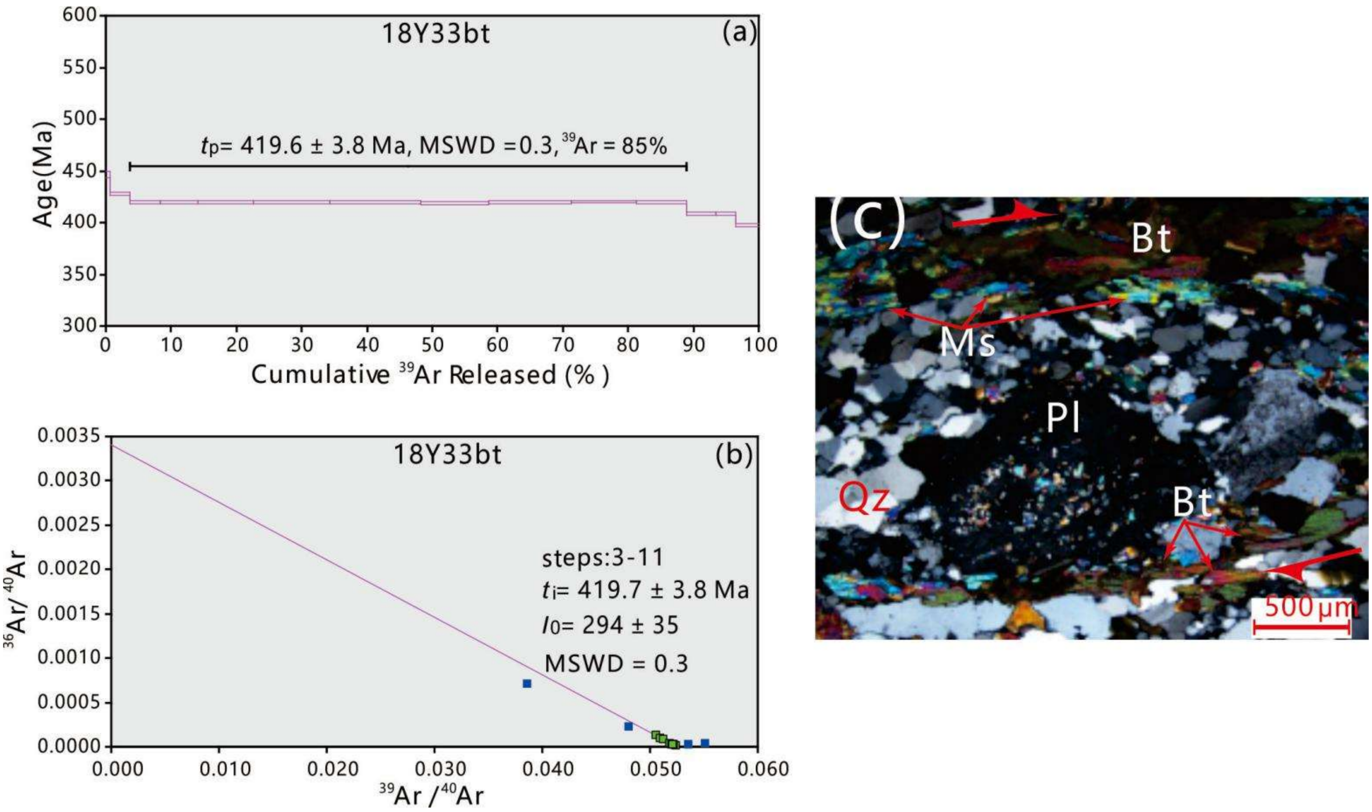

Figure 6. (**a**) Age spectrum and (**b**) inverse isochron for biotite (18M33Bt) from the mylonitic granite obtained by laser stepwise heating. (**c**) σ-type fabric and core–mantle structure of a (Pl) plagioclase porphyroblast surrounded by dynamically recrystallized (Ms) muscovite and (Bt) biotite, which are indicative of dextral shear.

5.3. Cassiterite Chemistry

The cassiterite high-field-strength elements is (Sc = 0.02–1.45 ppm; V = 1.62–9.50 ppm; Nb = 0.51–5.46 ppm; Ta = 0.01–1.09 ppm; Hf = 0–1.11 ppm; U = 0.02–0.46 ppm; Th = 0–0.02 ppm; Ti = 32.84–423.15 ppm; Pb = 0.01–8.11 ppm and Sb =9.92–56.45 ppm). Rare earth element (REE) concentrations are very low (total REE = 0.23–0.81 ppm). In chondrite-normalized REE diagrams, the cassiterite is enriched in light REEs and depleted in heavy REEs (Table 2).

Table 2. LA–ICP–MS trace element data for cassiterite in the Jialong Sn–Cu deposit, comparative data for cassiterite from other deposits are presented in Table 3.

Sample (ppm)	JL-1	JL-2	JL-3	JL-4	JL-5	JL-6	JL-7	JL-8
Sc	0.13	0.14	0.31	0.09	0.02	0.10	1.45	0.38
Ti	115.83	126.61	80.05	32.84	43.98	59.18	423.15	413.14
V	3.27	2.71	7.52	2.37	1.62	2.16	9.50	5.85
Cr	1.71	2.37	2.74	0.38	0.31	0.12	0.89	1.26
Mn	0.79	0.82	4.96	0.26	0.66	0.00	0.00	0.19
Fe	109.81	21.23	438.87	26.67	22.74	29.07	117.62	75.72
Cu	0.00	0.00	0.01	0.42	0.00	0.75	66.11	0.35
Zn	0.07	0.01	3.62	0.08	0.12	0.08	8.41	0.72
Nb	1.34	0.51	2.47	2.46	3.64	2.31	3.85	5.46
Mo	0.03	0.00	0.05	0.00	0.01	0.03	0.00	0.03
Cd	0.12	0.06	0.02	0.05	0.13	0.06	0.06	0.01
In	0.25	0.00	0.33	0.25	0.20	0.21	1.14	0.45
Sb	19.56	19.42	12.69	9.92	16.68	22.55	30.50	56.45
Hf	0.00	0.00	0.01	0.00	0.00	0.00	1.11	0.11
Ta	0.03	0.03	0.02	0.03	0.01	0.02	1.09	0.08
W	13.48	5.45	5.66	4.90	4.67	12.46	6.07	10.11
Pb	0.06	0.03	7.01	0.48	0.01	0.37	8.11	0.95
Th	0.00	0.00	0.00	0.00	0.01	0.00	0.02	0.01
U	0.02	0.03	0.10	0.11	0.13	0.19	0.40	0.46
ΣREE	0.24	0.27	0.36	0.39	0.81	0.24	0.42	0.38

6. Discussion

6.1. Caledonian Tin Mineralization

South China is one of the most important Sn ore provinces worldwide [2,36]. Sn mineralization occurred mainly in the Yanshanian, Jurassic, Neoproterozoic, and Indosinian periods. The U–Pb age of cassiterite from the Jialong Sn–Cu deposit is 421.9 ± 5.0 Ma, which confirms that Caledonian Sn mineralization occurred in this region. This age supports the hypothesis of Mao (1988) that the Caledonian orogeny led to the migration of Sn in Neoproterozoic strata and mafic–ultramafic igneous rocks, and the formation of Caledonian Sn deposits.

6.2. Trace Element Constraints on the Source of Ore-Forming Materials

Most global Sn mineralization is thought to be associated with highly differentiated and relatively reduced granitic magmatism [37,38]. Tin mineralization in northern Guangxi was not only closely related to Neoproterozoic granitoids, but also mafic–ultramafic igneous rocks [39–41]. The granites in the Jiuwandashan area are mainly middle Neoproterozoic in age [20,22,25–28]. After folding of the Neoproterozoic Sibao Group, magma was intruded along faults, which formed mafic–ultramafic intrusions and the Motianling, Yuanbaoshan, and other large granitic plutons in the Jiuwandashan area [33]. Previous studies have shown that Neoproterozoic subduction materials were reactivated and formed a series of mafic igneous rocks during late Mesozoic extension [42]. No other magmatism has been identified in or near the study area.

Cassiterite in Sn deposits related to granites has high concentrations of high-field-strength elements, such as W (12,000 ppm), Ti (2700 ppm), Nb (70 ppm), and Ta (4 ppm), as is the case for cassiterite in the Jiumao Sn deposit [43]. These characteristics are inherited from the magmatic–hydrothermal system of the granite. However, Sn deposits related to sedimentary or metamorphic fluid systems have low contents of high-field-strength elements. For example, the Yunlong Sn deposit in Yunnan Province, which is related to metamorphic rocks, has low contents of high-field-strength elements [44]. The Zr, Ti, Nb, Ta, and Sc contents of cassiterite in the Jialong deposit are low, but the contents of low-temperature, ore-forming elements (e.g., Pb and Sb) are obviously higher than those of the Jiumao Sn deposit. The contents of medium- to high-temperature elements (e.g., W, Zn, and

In) are lower than those of the Jiumao Sn deposit (Table 3). The trace element composition of cassiterite in the Jialong deposit is very different to that of magmatic cassiterite, but similar to that of cassiterite formed at low temperatures. This result, and the fact that the Sn mineralization age does not coincide with magmatism, indicates the Jialong deposit was not related to the magmatic–hydrothermal system of the Yuanbaoshan granite, and may have formed from a cooler fluid system.

Table 3. Comparison of cassiterite trace element contents for the Jialong Sn–Cu and Neoproterozoic Sn deposits in the Jiuwandashan area.

Elements	Jiumao Greisen Type			Jiumao Schist Type			Jiumao Amphibolite Type			Jialong		
	Average	Min.	Max.	Average	Min.	Max.	Average	Min.	Max.	Average	Min.	Max.
Sc	14.0	1.1	52.2	84.5	2.8	397.8	140.5	0.1	489.6	0.3	0.0	1.5
Ti	1144.1	29.2	2729.8	400.2	6.7	1227.2	405.6	1.4	1914.9	161.9	32.8	413.14
V	23.4	1.0	118.8	33.0	1.2	158.1	69.9	0.0	420.4	4.4	1.6	9.5
Mn	9.9	0.0	68.6	10.5	0.2	66.6	1.1	0.0	4.1	1.0	0.0	5.0
Fe	837.3	274.3	2188.9	1601.7	370.9	5177.8	371.3	54.3	936.8	105.2	21.2	438.9
Cu	2.4	0.0	9.0	1.5	0.1	5.5	33.9	0.0	148.7	8.5	0.0	66.1
Zn	58.5	0.3	142.4	35.5	4.6	83.4	18.7	0.0	64.3	1.5	0.0	8.4
Nb	10.9	0.6	70.8	0.7	0.0	4.0	0.2	0.0	1.0	2.8	0.5	5.5
In	6.5	0.1	16.7	74.8	10.7	137.2	913.3	39.6	2260.6	0.4	0.0	1.1
Sb	0.0	0.0	0.5	12.4	5.3	35.2	11.4	1.9	47.8	23.5	9.9	56.5
Ta	0.6	0.0	3.5	0.0	0.0	0.2	0.0	0.0	0.0	0.2	0.0	1.1
W	2131.2	0.9	1171.3	2312.4	133.3	5885.5	24.5	0.6	131.7	7.9	4.7	13.5
Pb	1.0	0.0	4.3	0.3	0.0	1.4	0.1	0.0	0.3	2.1	0.0	8.1
U	0.8	0.0	3.4	0.3	0.1	1.1	0.1	0.0	0.3	0.2	0.0	0.5
ΣREE	3.2	1.8	6.5	2.2	1.3	3.3	2.4	1.9	5.1	0.4	0.2	0.8
References	Xiang et al., (2018) [43]									This study		

6.3. Temporal and Spatial Relationships between Jialong Tin Mineralization and Ductile Shearing

Using the Riedel shear fracture theory, Roberts (1987) [45] identified five types of mineral-bearing fracture systems in ductile shear zones (R, R′, T, D, and P). The T and R fractures and R′ structures are important ore-bearing structures in shear zone-type ore deposits [46,47]. Faults in the Jialong deposit are mostly NE–SW- and NW–SE-trending, and the latter (interlayer) faults control the orebody distribution. Lenticular quartz and arsenopyrite veins, S–C fabrics (Figure 3d), mica fish (Figure 3c), rotational features, and dynamic quartz recrystallization show that the ductile shear zone underwent sinistral shear. Lenticular cassiterite grains also occur in the banded quartz aggregates and broken or granular cassiterite is enclosed by banded quartz (Figure 3e–f). This indicates that the cassiterite also experienced plastic deformation.

The Jialong deposit is located in the Sirong ductile shear zone on the eastern side of the Yuanbaoshan granite. The deposit was formed at 421.9 ± 5.0 Ma and the Sirong ductile shear zone was active at 419.6 ± 3.8 Ma, which shows that mineralization coincided with activity on the ductile shear zone. Cassiterite in the Jialong deposit exhibits obvious shear deformation, crushing, dissolution, and regrowth, suggesting that Sn mineralization was closely related to the Caledonian ductile shear zone.

Previous studies have found that when the $fo_2 < -40$ of ore-forming fluids and the pH < 4.0, early crystallized cassiterite can be dissolved at 250 °C and migrate as $SnCl_3^-$ [48]. Guo (2017) determined the deformation temperature of the Yuanbaoshan and Sirong ductile shear zones and suggested that ductile deformation occurred at medium–high temperatures (500 °C). The Sn contents of the Yuxi Formation in the Sibao Group (13.1 ppm) and Baizhu Formation in the Danzhou Group (11.7 ppm) are much higher than the average Sn content of continental crust (2 ppm), suggesting these rocks could have provided the materials for Sn mineralization [14].

Therefore, the Sirong ductile shear zone and secondary shear structures had a key role in controlling the shape, occurrence, size, and distribution of the Sn orebody. The active ductile shear zone may have provided the heat for the ore-forming hydrothermal system, and the NE–SW-trending T-fractures (i.e., secondary faults related to the sinistral ductile shear) provided space for the ore-forming fluids, depressurization, and mineralization.

6.4. Model of Caledonian Tin Mineralization

NW–SE compression occurred in the Jiuwandashan area during the early Paleozoic, which formed a series of large-scale, NE–SW-trending shear zones and released a large amount of hydrothermal fluids. NW–SE-trending brittle fractures were generated during this process, which provided migration channels for the ore-forming hydrothermal fluids and accommodation space for mineralization. During ductile deformation, under low-oxygen-fugacity and acidic fluid conditions, Sn was extracted from the country rocks by shearing-related metamorphic hydrothermal fluids. These Sn-rich fluids migrated along the NW–SE-trending brittle fractures and, as the pressure decreased, the fluid oxygen fugacity increased gradually due to continuous water–rock reactions. The fluid pH also increased and the activity of HCl decreased, which led to a lower solubility of Sn and other metallic elements in the fluid and, finally, ore precipitation and mineralization (Figure 7). Therefore, we propose that the Jialong Sn–Cu deposit was closely related to the Sirong ductile shear zone. This deposit is the first example of Caledonian and shear zone-related Sn mineralization identified in the Jiuwandashan area of northern Guangxi.

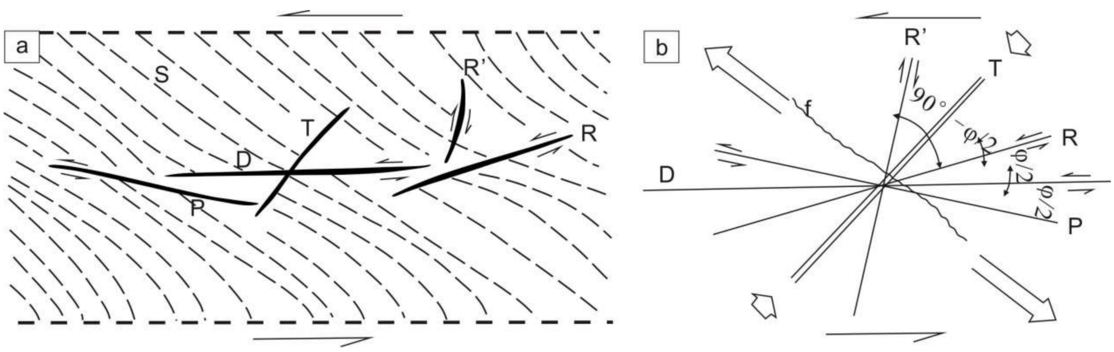

Figure 7. Shear zone features of the Sn ore-forming system [49,50] (modified after Aydin and Page, 1984; Sylvester, 1988). (**a**) Ore-bearing veins. (**b**) Shear fracture system. T = tension fissure formed along the strain ellipsoid (X–Z plane); R = Riedel shear; R′ = conjugate Riedel shear; S = foliation; D = principal shear fracture (i.e., parallel to the shear zone boundary); f = fold surface; P = co-shear fracture; φ = angle of internal friction.

7. Conclusions

The Jialong Sn–Cu deposit has a cassiterite U–Pb age of 421.9 ± 5.0 Ma and is the first Caledonian Sn mineralization discovered in the Jiuwandashan area of northern Guangxi. Cassiterite in the Jialong deposit is strongly depleted in Nb, Ta, Ti, Sc, Hf, and other high-field-strength elements, and relatively enriched in low-temperature elements, such as Pb and Sb. These features are typical of non-magmatic cassiterite. There was also no coeval magmatism in this region, indicating that the Jialong deposit was not directly related to magmatism, and that Sn and other ore-forming materials were derived from Sn-rich Neoproterozoic strata. The Jialong deposit is located in the northeastern part of the Sirong ductile shear zone and exhibits shear deformation, which controlled the Sn orebody. The ductile shear zone may have provided the heat and materials for the ore-forming hydrothermal fluids. NW–SE-trending T fractures provided favorable space for the mineralizing fluids. The Jialong deposit was closely temporally and spatially related to a Caledonian ductile shear zone. Cassiterite is sheared, fractured, and exhibits dissolution and regrowth. This indicates that shear-related, metamorphic, hydrothermal fluids generated by Caledonian tectonism extracted Sn from Sn-rich strata, and then migrated along interlayer faults produced by shear deformation. With decreasing pressure and continuous water–rock reactions, Sn and other metal elements became insoluble in the fluids and mineralization occurred.

Author Contributions: Conceptualization, Z.-H.Y. and L.-A.B.; methodology, Z.-H.Y.; software, Z.-H.Y.; validation, L.-A.B., R.-G.H., J.W., Z.-H.F. and C.X.; formal analysis, L.-A.B.; investigation, L.-A.B.; resources, L.-A.B.; data curation, Z.-H.Y.; writing—original draft preparation, Z.-H.Y.; writing—review and editing, Z.-H.Y.; visualization, Z.-H.Y.; supervision, Z.-X.Z., X.-J.L. and Y.D.; project administration, Y.D. and S.-Y.Z.; Data curation Z.-X.Z.; funding acquisition, L.-A.B. All authors have read and agreed to the published version of the manuscript.

Funding: This research was supported by the National Natural Science Foundation of China (Grant 42072259 and 42162008), the Guangxi Natural Science Foundation (Grants 2019GXNSFDA245009, 2020GXNSFAA297049 and 2021JJA150058), and a preliminary project fund from the Guangxi Bureau of Geology and Mineral Resources in 2018 (Guilin Geology and Mining Comprehensive Research Institute [2018] No. 14).

Data Availability Statement: The data that support the findings of this study are available on request from the corresponding author. The data are not publicly available due to privacy or ethical restrictions.

Conflicts of Interest: We declare that we do not have any commercial or associative interest that represents a conflict of interest in connection with the work submitted.

References

1. Heinrich, C.A. The chemistry of hydrothermal tin(-tungsten) ore deposition. *Econ. Geol.* **1990**, *85*, 457–481. [CrossRef]
2. Lehmann, B. *Metallogeny of Tin*; Springer: Berlin, Germany, 1990; p. 211.
3. Mao, J.W.; Xie, G.Q.; Guo, A.L.; Yuan, S.D.; Cheng, Y.B.; Chen, Y.C. Spatial-Temporal distribution of mesozoic ore deposits in South China and their metallogenic settings. *Geol. J. China Univ.* **2008**, *14*, 510–526.
4. Li, X. Micro-Geochemical Analysis and Metallogenic Mechanism of Tin-Copper Associated Deposits: Case Studies of the Neves Corvo Deposit in Portugal and the Gejiu Deposit in Yunnan, China. Ph.D. Thesis, China University of Geosciences, Wuhan, China, 2020; p. 150.
5. Yu, J.M.; Jiang, S.Y.; Pan, J.Y.; Ni, P.; Ling, H.F. Evolution of Ore-forming fluids in the Yunlong tin deposit, Western Yunnan: Evidence from Hydrogen and Oxygen isotopes. *Geol. Rev.* **2002**, *48*, 250–255.
6. Yu, J.M.; Jiang, S.Y. Trace element geochemistry of cassiterite from the Neves Corvo massive sulfide deposit, Portugal. *Geochimica* **2001**, *30*, 140.
7. Marignac, C.; Cathelineau, M. Comment on the paper by Sanchez-España et al.: Source and evolution of ore-forming hydrothermal fluids in the northern Iberian pyrite belt massive sulphide deposits (SW Spain): Evidence from fluid inclusions and stable isotopes (Mineralium Deposita 38: 519–537). *Miner. Depos.* **2006**, *40*, 742–748.
8. Moura, A. Metallogenesis at the Neves Corvo VHMS deposit (Portugal): A contribution from the study of fluid inclusions. *Ore Geol. Rev.* **2008**, *34*, 354–368. [CrossRef]
9. Hua, R.M.; Chen, P.R.; Zhang, W.L.; Liu, X.D.; Lu, J.J.; Lin, J.F.; Yao, J.M. Preliminary Study on Mesozoic and Cenozoic Ore-forming Systems Related to Granitic Magmatism South China. *Natl. Conf. Miner. Depos. 7th Xian China* **2002**, *2002*, 132–135.
10. Hua, R.M.; Zhang, W.L.; Gu, S.Y.; Chen, P.R. Comparison between REE granite and W-Sn granite in the Nanling region, South China, and their mineralizations. *Acta Geol. Sin.* **2007**, *23*, 2321–2328.
11. Mao, J.W.; Xie, G.Q.; Guo, C.L.; Chen, Y.C. Large-scale tungsten-tin mineralization in the Nanling region, South China: Metallogenic ages and corresponding geodynamic processes. *Acta Petrol. Sin.* **2007**, *23*, 2329–2338.
12. Mao, J.W.; Xie, G.Q.; Chen, Y.B.; Chen, Y.C. Mineral deposit models of Mesozoic ore deposits in South China. *Geol. Rev.* **2009**, *55*, 347–354.
13. Mao, J.W.; Ouyang, H.G.; Song, S.W.; Santosh, M.; Yuan, S.D.; Zhou, Z.H.; Zheng, W.; Liu, H.; Liu, P.; Cheng, Y.B. Geology and metallogeny of tungsten and tin deposits in China. *SEG Spec. Publ.* **2019**, *22*, 411–482.
14. Chen, J. *Geochemistry of Tin*; Nanjing University Press: Nanjing, China, 2000; p. 320.
15. Rudnick, R.L.; Gao, S.; Holland, H.D. Composition of the continental crust. *Crust* **2003**, *3*, 1–64.
16. BGMRGX (Bureau of Geology and Mineral Resources of Guangxi Province). *Regional Geology of Guangxi Autonomous Region*; Geological Publishing House: Beijing, China, 1985; pp. 1–853. (In Chinese)
17. Zhu, L.J.; Du, D.Q. Low-temperature deformation and metallogenesis at Jiumao tin deposit, Guangxi. *Dep. Geol. Guizhou Inst. Technol.* **1994**, *1*, 90–93.
18. Mao, J.W. Igneous Rock Series and Metallogenic Series of Tin Polymetallic Deposits in Jiuwandashan-Yuanbaoshan Region, North Guangxi. Ph.D. Thesis, Chinese Academy of Geological Sciences, Beijing, China, 1988; p. 209.
19. Chen, Y.C.; Mao, J.W. The evolutionary history of metallic deposits in Northern Guangxi. *China Acta Geol. Sin.* **1994**, *68*, 324–338.

20. Li, X.H.; Liu, Y. Multiple-stage evolution of zircon U-Pb isotopic systematics in S-type granites and its chronological significance:A case study on Sanfang granite, Northern Guangxi. *Acta Geol. Sin.* **1996**, *16*, 169–177.
21. Li, X.H. U–Pb zircon ages of granites from the southern margin of the Yangtze Block: Timing of Neoproterozoic Jinning: Orogeny in SE China and implications for Rodinia Assembly. *Precambrian Res.* **1999**, *97*, 43–57. [CrossRef]
22. Wang, X.L.; Zhou, J.C.; Qiu, J.S.; Zhang, W.L.; Liu, X.M.; Zhang, G.L. LA-ICP-MS U-Pb zircon geochronology of the Neoproterozoic igneous rocks from Northern Guangxi, South China: Implications for tectonic evolution. *Precambrian Res.* **2006**, *145*, 111–130. [CrossRef]
23. Wang, X.L.; Zhou, J.C.; Griffin, W.L.; Zhao, G.; Yu, J.H.; Qiu, J.S.; Zhang, Y.J.; Xing, G.F. Geochemical zonation across a Neoproterozoic orogenic belt: Isotopic evidence from granitoids and metasedimentary rocks of the Jiangnan orogen, China. *Precambrian Res.* **2014**, *242*, 154–171. [CrossRef]
24. Gao, L.Z.; Dai, C.G.; Liu, Y.X.; Wang, M.; Wang, X.H.; Chen, J.S.; Ding, X.Z.; Zhang, C.H.; Cao, Q.; Liu, J.H. Zircon SHRIMP U-Pb dating of tuff bed of the Sibao Group in southeastern Guizhou-northern Guangxi area, China and its stratigraphic im-plication. *Geol. Bull. China* **2010**, *29*, 1259–1267.
25. Zhang, S.T.; Ma, D.S.; Lu, J.J.; Zhang, R.Q.; Cai, Y.; Ding, C.C. Geochronology, Hf isotopic compositions and geochemical characteristics of the Pingying granite pluton in Northern Guangxi, South China, and its geological significance. *Geol. J. China Univ.* **2016**, *22*, 92–104.
26. Guo, A.L. Tectonic Characteristics and Rheological Parameter Estimation of Yuanbaoshan Ductile Shear Zone. Master's Thesis, Guilin University of Technology, Guilin, China, 2017; p. 80.
27. Zhang, G.L. Kinematics and Dynamics of Pre-Devonian Tectonic Evolution at South, Margin of Yangtze Block in North Guangxi. Ph.D. Thesis, Central South University, Hunan, China, 2004; p. 193.
28. Chen, L.; Wang, Z.Q.; Yan, Z.; Gong, J.H.; Ma, S.X. Zircon and cassiterite U-Pb ages, petrogeochemistry and metallogenesis of Sn deposits in the Sibao area, northern Guangxi: Constraints on the neoproterozoic granitic magmatism and related Sn mineralization in the western Jiangnan Orogen, South China. *Mineral. Petrol.* **2018**, *112*, 437–463. [CrossRef]
29. Dai, Y.; Lu, G.; Feng, Z.H.; Li, S.H. The relationship between shear zone and tin mineralization in Jiuwangdashan area, northern Guangxi. *Nanning Print. House Geol. Inst. Guangxi Bur. Geol. Miner. Resour.* **2020**, *1*, 30–79.
30. Zhang, S.T.; Zhang, R.Q.; Lu, J.J.; Ma, D.S.; Ding, T.; Gao, S.Y.; Zhang, Q. Neoproterozoic tin mineralization in South China: Geology and cassiterite U–Pb age of the Baotan tin deposit in northern Guangxi. *Miner. Depos.* **2019**, *54*, 1125–1142. [CrossRef]
31. Li, S.S.; Feng, Z.H.; Qin, Y.; Pang, C.J.; Wang, C.Z. The relationship between ductile shear zone and mineralization in the Jiufeng Sn deposit, northern Guangxi, South China: Evidence from structural analysis and cassiterite U-Pb dating. *Ore Geol. Rev.* **2020**, *124*, 103655. [CrossRef]
32. Zhang, X.F.; Meng, X.G.; Han, J.E.; Shao, Z.G.; Zhang, D. Discovery of the ductile shear zone in the Sibao area of northern Guangxi and its tectonic significance. *Acta Geosci. Sin.* **2015**, *36*, 161–167.
33. Yan, C.L.; Shu, L.S.; Chen, Y.; Michel, F.; Feng, Z.H.; Zhai, M.G. The construction mechanism of the Neoproterozoic S-type Sanfang-Yuanbaoshan granitic plutons in the Jiangnan Orogenic Belt, South China: Insights from geological observation, geochronology, AMS and Bouguer gravity modeling. *Precambrian Res.* **2021**, *354*, 106054. [CrossRef]
34. Bai, Y.M. Relationship between Ductile Shear Zone and Tin Mineralization in Jiuwandashan Area, Northern Guangxi. Master's Thesis, Guilin University of Technology, Guilin, China, 2019; p. 97.
35. Slack, J.F.; Neymark, L.A.; Moscati, R.J.; Lowers, H.A.; Ransom, P.W.; Hauser, R.L.; Adams, D.T. Origin of Tin Mineralization in the Sullivan Pb-Zn-Ag Deposit, British Columbia: Constraints from Textures, Geochemistry, and LA-ICP-MS U-Pb Geochronology of Cassiterite. *Econ. Geol.* **2020**, *115*, 1125–1142. [CrossRef]
36. Hua, R.M.; Li, G.L.; Zhang, W.L.; Hu, D.Q.; Chen, P.R.; Chen, W.F.; Wang, X.D. A tentative discussion on differences between large-scale tungsten and tin mineralizations in South China. *Miner. Depos.* **2010**, *29*, 9–23.
37. Groves, D.I.; Mccarthy, T.S. Fractional crystallization and the origin of tin deposits in granitoids. *Miner. Depos.* **1978**, *13*, 11–26. [CrossRef]
38. Lehmann, B. Tin granites, geochemical heritage, magmatic differentiation. *Geol. Rundsch.* **1987**, *76*, 177–185. [CrossRef]
39. Lin, J.J.; Ma, F.J.; Yang, K.T.; Wang, R.C.; Mao, J.W.; Tang, S.H. Study on geochemistry and geology of stable isotope in Baotan tin deposit, Guangxi. *Geol. Guangxi* **1986**, *2*, 23–31.
40. Mao, J.W.; Lin, J.J.; Ma, F.J. The genesis of the Yidong-Wudi tin deposit, Guangxi. *Geol. Rev.* **1987**, *33*, 547–558.
41. Chen, J. Tin minerlization in metavolcanoclastic and metaultramafic rocks of the Jiumao mine, Northern Guangxi, South China. *Sci. Geolodica Sin.* **1995**, *4*, 21–31.
42. Su, H.M.; Jiang, S.Y.; Shao, J.B.; Zhang, D.Y.; Huang, X.Q. New identification and significance of Early Cretaceous mafic rocks in the interior South China Block. *Sci. Rep.* **2021**, *11*, 11396. [CrossRef]
43. Xiang, L.; Wang, R.C.; Erdmann, S.; Sizaret, S.; Lu, J.J.; Zhang, W.L.; Xie, L.; Che, X.D.; Zhang, R.Q. Neoproterozoic mineralization in a hydrothermal cassiterite-sulfide deposit at Jiumao, northern Guangxi, South China: Mineral-scale constraints on metal origins and ore-forming processes. *Ore Geol. Rev.* **2018**, *94*, 172–192. [CrossRef]
44. Jiang, S.Y.; Yu, J.M.; Lu, J.J. Trace and rare-earth element geochemistry in tourmaline and cassiterite from the Yunlong tin deposit, Yunnan, China: Implication for migmatitic–hydrothermal fluid evolution and ore genesis. *Chem. Geol.* **2004**, *209*, 193–213. [CrossRef]
45. Roberts, R.G. Ore deposit models Archean lode gold deposits. *Geosci. Can.* **1987**, *14*, 37–52.

46. Deng, J.; Zhai, Y.S.; Yang, L.Q. On ore-forming system of shear zone tectonics. *Geoscience* **1998**, *12*, 493–500.
47. Hou, Q.L.; Liu, Q. *Tectonic Conditions and Mechanochemical Process of Mineralzation of Shear Zone Type Deposits*; Science Press: Beijing, China, 2020; p. 175.
48. Cooke, D.R.; Bull, S.W.; Large, R.R.; McGoldrick, P.J. The importance of oxidized brines for the formation of Australian Proterozoic stratiform sediment-hosted Pb-Zn (Sedex) deposits. *Econ. Geol.* **2000**, *95*, 1–18. [CrossRef]
49. Aydin, A.; Page, B.M. Diverse Pliocene-Quaternary tectonics in a transform environment, San Francisco Bay region, California. *Geol. Soc. Am. Bull.* **1984**, *95*, 1303–1317. [CrossRef]
50. Sylvester, A.G. Strike-slip faults. *Geol. Soc. Am. Bull.* **1988**, *100*, 1666–1703. [CrossRef]